

Two-Mirror Apodization for High-Contrast Imaging

Wesley A. Traub

Harvard-Smithsonian Center for Astrophysics

wtraub@cfa.harvard.edu

and

Robert J. Vanderbei

Operations Research and Financial Engineering, Princeton University

rvdb@princeton.edu

ABSTRACT

Direct detection of extrasolar planets will require imaging systems capable of unprecedented contrast. Apodized pupils provide an attractive way to achieve such contrast but they are difficult, perhaps impossible, to manufacture to the required tolerance and they absorb about 90% of the light in order to create the apodization, which of course lengthens the exposure times needed for planet detection. A recently proposed alternative is to use two mirrors to accomplish the apodization. With such a system, no light is lost. In this paper, we provide a careful mathematical analysis, using one dimensional mirrors, of the on-axis and off-axis performance of such a two-mirror apodization system. There appear to be advantages and disadvantages to this approach. In addition to not losing any light, we show that the nonuniformity of the apodization implies an extra magnification of off-axis sources and thereby makes it possible to build a real system with about half the aperture that one would otherwise require or, equivalently, resolve planets at about half the angular separation as one can achieve with standard apodization. More specifically, ignoring pointing error and stellar disk size, a planet at $1.7\lambda/D$ ought to be at the edge of detectability. However, we show that the non-zero size of a stellar disk pushes the threshold for high-contrast so that a planet must be at least $2.5\lambda/D$ from its star to be detectable. The off-axis analysis of two-dimensional mirrors is left for future study.

Subject headings: Extrasolar planets, coronagraphy, point spread function, apodization

1. Introduction

In a recent paper, Goncharov et al. (2002) propose using two mirrors to convert a uniform-intensity beam to one of nonuniform intensity—that is, an apodized exit beam. The motivation for their work was to “mask” the secondary mirror in designs of large two-mirror telescopes with fast spherical primaries. As an application of the idea, they point to radio and submillimeter-wave telescopes since for these it is important to suppress sidelobes and reduce background noise. However, its applicability to high-contrast imaging in the context of the Terrestrial Planet Finder (TPF) project immediately caught our attention and the result is the work described in this paper.

Independently of Goncharov et. al., Guyon (2003) studied the same two-mirror apodization idea and analyzed its applicability to extra-solar planet finding. His work was motivated by Labeyrie’s paper on pupil densification (Labeyrie (1996)). The idea behind pupil densification is to reduce the intensity of the diffraction side lobes by remapping the sparse input pupil of an interferometer to a more compact exit pupil. Pupil densification provides the advantage of a better-concentrated image at the cost of field of view, since it violates the “golden rule” of combining beams (Traub (1986)); this rule states that, to provide a large field of view, the exit pupil of an optical system must be a scaled version of the input pupil. Since pupil densification is a special case of pupil remapping, both will suffer field of view loss if the scaling factor is not constant.

Nevertheless, the potential gains from pupil mapping are so significant that it is worthwhile exploring this technique for the purpose of extrasolar planet searching, and this is the goal of the present paper.

In his paper, Guyon argues that the two-mirror approach provides a system with (i) a smaller inner working angle ($1\lambda/D$ vs. $4\lambda/D$) and consequently a smaller overall aperture and (ii) a higher throughput with a corresponding reduction in exposure time. Here, and throughout the paper, λ is wavelength and D is the diameter of the primary mirror. Guyon also addresses, at least qualitatively, the issue of off-axis performance of the system.

In this paper, we give a careful mathematical analysis of the on-axis and off-axis performance of this two-mirror system. We deal exclusively with one-dimensional mirrors in two-dimensional space. While the on-axis analysis is easily extended to real two-dimensional mirrors in three space dimensions, the off-axis analysis, which is the crux of this paper, is much more difficult in this higher dimension. Hence, we leave such analysis to future work.

The first and most obvious advantage of the two-mirror system is that throughput is increased since no light is lost. Furthermore, an interesting and unexpected advantage of this system is that there is an inherent magnification introduced by a nonuniform apodization. For example, a planet at $5\lambda/D$ in the sky actually appears at about $12\lambda/D$ in the image plane. This improves the effective inner working angle by a factor of 2.4 and explains, we believe, Guyon’s claims about improved

inner working angle. Consequently, such a system for planet finding could be implemented with a smaller mirror than would otherwise be required or, equivalently, could detect planets less than half as far from their parent star with the same aperture.

There is, however, a downside. We show that the inner working angle of an ideal system (with an on-axis source) is still $4\lambda/D$ and furthermore that even tiny off-axis light sources, such as arising from the nonzero size of the stellar disk, increase the inner working angle to at least $6\lambda/D$. So, a star at $2.5\lambda/D$ in the sky will appear at $6\lambda/D$ in the image plane and hence lie on the edge of detectability. This still represents a significant improvement over the $4\lambda/D$, which is the best one can do with standard apodization or with pupil masks.

In the next section, we derive the basic equations relating the shapes of two one-dimensional mirrors to the apodization they produce. Then, in Section 3, we give a careful analysis of the off-axis performance of this two-mirror system. Section 4 then goes through some specific examples, including the case of two parabolas, where everything can be computed explicitly. Finally, in Section 5, we show the results of numerical computations using the known optimal apodizer.

We end the present section with a word about our notation. Given any function of a single real variable, we use a prime to denote the derivative of this function with respect to its variable. So, for example, $h'(x) = dh(x)/dx$.

2. Mirror-Based Apodization

Figure 1 illustrates the use of two mirrors to produce an apodization. Parallel light rays come down from above, reflect off the bottom mirror (on the left), bounce up to the top mirror (on the right), and then exit downward as a parallel bundle with a concentration of rays in the center of the bundle and thinning out toward the edges—that is, the exit bundle is apodized. A focusing element on the x -axis then creates an image.

Let $h(x)$, $a \leq x \leq b$, denote the height-function defining the lower mirror and let $g(\tilde{x})$, $-\frac{d}{2} \leq \tilde{x} \leq \frac{d}{2}$, denote the height-function defining the upper mirror. We suppose there is a one-to-one correspondence between x 's in the interval $[a, b]$ and the interval $[-\frac{d}{2}, \frac{d}{2}]$ that is determined by the desired apodization. Let $\tilde{x}(x)$ denote the value in $[-\frac{d}{2}, \frac{d}{2}]$ associated with x in $[a, b]$. We assume that the function \tilde{x} , which we call the *transfer function*, is strictly monotone (either increasing or decreasing). It then has a functional inverse. Let $x(\tilde{x})$ denote this inverse function. The *apodization* $A(\cdot)$ associated with this correspondence is given by

$$\frac{dx}{d\tilde{x}}(\tilde{x}) = A(\tilde{x}). \quad (1)$$

Adding a boundary condition, such as $x(-\frac{d}{2}) = a$, makes it possible to derive the correspondence

from the apodization.

The shapes of the two mirrors are determined by enforcing equality between angle-of-incidence and angle-of-reflection (i.e., Snell's law) at the two mirror surfaces. The tangent vector to the first mirror is $(1, h'(x))$. The unit incidence vector is $(0, 1)$ and the unit reflection vector is $(\tilde{x} - x, g(\tilde{x}) - h(x))/S(x, \tilde{x})$, where

$$S(x, \tilde{x}) = \sqrt{(\tilde{x} - x)^2 + (g(\tilde{x}) - h(x))^2} \quad (2)$$

denotes the distance between the point $(x, h(x))$ on the first mirror and $(\tilde{x}, g(\tilde{x}))$ on the second mirror. The scalar product between the tangent vector and the unit incidence vector must be equal to the negative of the scalar product between the tangent vector and the unit reflection vector. Equating these inner products, we get the following differential equation for h :

$$h'(x) = \frac{x - \tilde{x}}{S(x, \tilde{x}) - h(x) + g(\tilde{x})}. \quad (3)$$

Applying the same technique to the surface of the second mirror at \tilde{x} , we get the same expression for g' and so

$$g'(\tilde{x}) = h'(x). \quad (4)$$

Equation (4) says that, for a given ray, the slopes of the mirrors are locally the same, which is to be expected since the input ray is parallel to the output ray. From equations (3) and (4), it appears that the differential equations for h and g are a coupled system of ordinary differential equations. Our first task is to show how to decouple them.

Let

$$P_0(x, \tilde{x}) = S(x, \tilde{x}) + g(\tilde{x}) - h(x), \quad (5)$$

denote the denominator in (3). It is the total *optical path length* from a point on any given horizontal line drawn above the first mirror (and below the second) vertically down to the first mirror diagonally up to the second mirror and finally vertically back down to the same horizontal line below the second mirror.

Theorem 1 *The optical path length P_0 is a conserved quantity for on-axis rays.*

Proof. If we regard x as a function of \tilde{x} and differentiate with respect to \tilde{x} , we get

$$\frac{d}{d\tilde{x}} (S(x, \tilde{x}) + g(\tilde{x}) - h(x)) = G(\tilde{x}) - H(\tilde{x}) \frac{dx}{d\tilde{x}}, \quad (6)$$

where

$$G(\tilde{x}) = \frac{\tilde{x} - x + (g(\tilde{x}) - h(x))g'(\tilde{x})}{S(x, \tilde{x})} + g'(\tilde{x}) \quad (7)$$

$$H(\tilde{x}) = \frac{\tilde{x} - x + (g(\tilde{x}) - h(x))h'(x)}{S(x, \tilde{x})} + h'(x). \quad (8)$$

From (4), we see that $G(\tilde{x}) = H(\tilde{x})$. Using (3) to eliminate $h'(x)$ from (8), we get after some straightforward algebraic manipulation that $H(\tilde{x}) = 0$ and therefore P_0 is a constant. \square

Henceforth, we write P_0 for this optical-path-length invariant.

Corollary 1 *The differential equations for h and g are decoupled:*

$$h'(x) = g'(\tilde{x}) = \frac{x - \tilde{x}}{P_0}. \quad (9)$$

Isolating $S(x, \tilde{x})$ on one side of the equation in (5) and squaring, we can solve for the difference between $g(\tilde{x})$ and $h(x)$:

$$g(\tilde{x}) - h(x) = -\frac{(\tilde{x} - x)^2}{2P_0} + \frac{P_0}{2}. \quad (10)$$

Hence, it is only necessary to solve one of the differential equations. The other mirror surface can then be computed from this difference.

3. Off-Axis Performance

Suppose now that coherent light enters at angle θ from on-axis as shown in Figure 2. The light that strikes at position $(x, h(x))$ on the first mirror reflects off at a different angle and strikes the second mirror at a new position shifted by $\Delta\tilde{x}$ from the on-axis strike point: $(\tilde{x} + \Delta\tilde{x}, g(\tilde{x} + \Delta\tilde{x}))$. Light then reflects off the second mirror at angle $\tilde{\theta}$ and intersects the x -axis at position $\tilde{\tilde{x}}$. We need to compute how $\Delta\tilde{x}$, $\tilde{\theta}$, and $\tilde{\tilde{x}}$ depend on θ with the ultimate goal of using these expansions to compute the image-plane point-spread function as a function of θ .

Lemma 1 $\Delta\tilde{x} = S(x, \tilde{x}) \theta + o(\theta)$.

Proof. The unit incidence vector is $(-\sin \theta, \cos \theta)$ and the unit reflection vector is $(\tilde{x} + \Delta\tilde{x} - x, g(\tilde{x} + \Delta\tilde{x}) - h(x))/S(x, \tilde{x} + \Delta\tilde{x})$. As before, Snell's law can be expressed by equating the inner product between the unit incidence vector and the mirror's tangent vector with the negative of the corresponding inner product for the unit reflection vector. We get that

$$-\sin \theta + h'(x) \cos \theta = -\frac{(\tilde{x} + \Delta\tilde{x} - x + h'(x)(g(\tilde{x} + \Delta\tilde{x}) - h(x)))}{S(x, \tilde{x} + \Delta\tilde{x})}. \quad (11)$$

Linearizing the left-hand side in θ and the right-hand side in $\Delta\tilde{x}$ and noting that the constant terms in the two linearizations match, since they give the on-axis equation satisfied by $h'(x)$, we get

$$\theta \approx \left(\frac{1 + h'(x)g'(\tilde{x})}{S(x, \tilde{x})} - \frac{\tilde{x} - x + h'(x)(g(\tilde{x}) - h(x))}{S(x, \tilde{x})^3} (\tilde{x} - x + g'(\tilde{x})(g(\tilde{x}) - h(x))) \right) \Delta\tilde{x}. \quad (12)$$

Using Corollary 1, the first term on the right simplifies to $(1 + h'(x)^2)/S(x, \tilde{x})$ and the second term simplifies to $h'(x)^2/S(x, \tilde{x})$. Hence, we get that to first order $\theta = \Delta\tilde{x}/S(x, \tilde{x})$ from which the lemma follows. \square

Lemma 2 $\tilde{\theta} = \frac{A(\tilde{x})}{S(x, \tilde{x})} \Delta\tilde{x} + o(\Delta\tilde{x}) = A(\tilde{x})\theta + o(\theta)$.

Proof. The proof is similar to that of the previous lemma. The unit reflection vector is $(\sin \tilde{\theta}, -\cos \tilde{\theta})$ and the unit incidence vector is just the negative of what it was before: $-(\tilde{x} + \Delta\tilde{x} - x, g(\tilde{x} + \Delta\tilde{x}) - h(x))/S(x, \tilde{x} + \Delta\tilde{x})$. The mirror's tangent vector at $\tilde{x} + \Delta\tilde{x}$ is $(1, g'(\tilde{x} + \Delta\tilde{x}))$. As before, Snell's law can be expressed by equating the inner product between the unit incidence vector and the mirror's tangent vector with the negative of the corresponding inner product for the unit reflection vector. We get that

$$\sin \tilde{\theta} - g'(\tilde{x} + \Delta\tilde{x}) \cos \tilde{\theta} = \frac{(\tilde{x} + \Delta\tilde{x} - x + g'(\tilde{x} + \Delta\tilde{x})(g(\tilde{x} + \Delta\tilde{x}) - h(x)))}{S(x, \tilde{x} + \Delta\tilde{x})}. \quad (13)$$

Linearizing both sides in $\tilde{\theta}$ and $\Delta\tilde{x}$ and noting that the constant terms in the two linearizations match, since they give the on-axis equation satisfied by $g'(\tilde{x})$, we now get after employing Corollary 1 that

$$\tilde{\theta} - g''(\tilde{x})\Delta\tilde{x} \approx \left(\frac{1 + g'(\tilde{x})^2 + (g(\tilde{x}) - h(x))g''(\tilde{x})}{S(x, \tilde{x})} - \frac{g'(\tilde{x})^2}{S(x, \tilde{x})} \right) \Delta\tilde{x}. \quad (14)$$

Moving $\Delta\tilde{x}$ terms to the right-hand side and simplifying, we get

$$\begin{aligned}\tilde{\theta} &= \frac{1 + g''(\tilde{x})(S(x, \tilde{x}) + g(\tilde{x}) - h(x))}{S(x, \tilde{x})} \Delta\tilde{x} \\ &= \frac{1 + g''(\tilde{x})P_0}{S(x, \tilde{x})} \Delta\tilde{x}\end{aligned}\quad (15)$$

Differentiating the expression for $g'(\tilde{x})$ given in Corollary 1, we get that

$$g''(\tilde{x}) = \frac{dx/d\tilde{x} - 1}{P_0} = \frac{A(\tilde{x}) - 1}{P_0}.\quad (16)$$

Substituting (16) into (15), we get the claimed first-order relationship between $\tilde{\theta}$ and $\Delta\tilde{x}$. The relationship between $\tilde{\theta}$ and θ then follows from Theorem 1. \square

From these expansions, we can compute the phase of the wavefront at the exit pupil or, equivalently, the path length from an isophase line at the entrance pupil through the system to the exit pupil. To this end, note that, for any y_0 , the line $y = y_0 + x \sin \theta$, $x \in [b, c]$, is an iso-phase line for the entering wave. Fix such a y_0 . Let $e(x, \theta)$ denote the length of the light ray from this line to the first mirror surface. The interval $[-\frac{d}{2}, \frac{d}{2}]$ of the x -axis can be regarded as an exit pupil. Let \tilde{x} denote the position along this pupil where the off-axis light beam exits the system. Let $f(x, \theta)$ denote the length of the light ray from $(\tilde{x} + \Delta\tilde{x}, g(\tilde{x} + \Delta\tilde{x}))$ to this point on the pupil. The path length from the iso-phase line to the exit pupil is

$$P(x) = e(x, \theta) + S(x, \tilde{x} + \Delta\tilde{x}) + f(x, \theta).\quad (17)$$

Theorem 2 $P(x) = P_0 + y_0 + x\theta + o(\theta)$.

Proof. Simple geometry reveals that

$$e(x, \theta) = y_0 - h(x) \cos \theta + x \sin \theta = y_0 - h(x) + x\theta + o(\theta)\quad (18)$$

and that

$$\begin{aligned}f(x, \theta) &= \frac{g(\tilde{x} + \Delta\tilde{x})}{\cos \tilde{\theta}} = g(\tilde{x}) + g'(\tilde{x})\Delta\tilde{x} + o(\Delta\tilde{x}) \\ &= g(\tilde{x}) + g'(\tilde{x})S(x, \tilde{x})\theta + o(\theta).\end{aligned}\quad (19)$$

We need a first-order expansion of $S(x, \tilde{x} + \Delta\tilde{x})$:

$$S(x, \tilde{x} + \Delta\tilde{x}) = S(x, \tilde{x}) + \frac{\tilde{x} - x + (g(\tilde{x}) - h(x))g'(\tilde{x})}{S(x, \tilde{x})} \Delta\tilde{x} + o(\Delta\tilde{x}). \quad (20)$$

From Corollary 1 and equation (5), we get that

$$\tilde{x} - x + (g(\tilde{x}) - h(x))g'(\tilde{x}) = (-P_0 + g(\tilde{x}) - h(x))g'(\tilde{x}) = -S(x, \tilde{x})g'(\tilde{x}). \quad (21)$$

Substituting this into (20) and using Theorem 1, we get

$$S(x, \tilde{x} + \Delta\tilde{x}) = S(x, \tilde{x}) - g'(\tilde{x})S(x, \tilde{x})\theta + o(\theta). \quad (22)$$

Adding terms and using (5), we get the claimed result. \square

Lemma 3 $\tilde{\tilde{x}} = \tilde{x} + (S(x, \tilde{x}) + g(\tilde{x})A(\tilde{x}))\theta + o(\theta)$.

Proof. Simple geometry followed by application of previously derived first-order expansions reveal that

$$\begin{aligned} \tilde{\tilde{x}} &= \tilde{x} + \Delta\tilde{x} + g(\tilde{x} + \Delta\tilde{x}) \tan \tilde{\theta} \\ &= \tilde{x} + \Delta\tilde{x} + (g(\tilde{x}) + g'(\tilde{x})\Delta\tilde{x})\tilde{\theta} + o(\tilde{\theta}) \\ &= \tilde{x} + (S(x, \tilde{x}) + g(\tilde{x})A(\tilde{x}))\theta + o(\theta). \end{aligned} \quad (23)$$

This completes the proof. \square

Now consider a focusing element placed over the interval $[-\frac{d}{2}, \frac{d}{2}]$ of the positive x -axis of focal length f as shown in Figure 1. The electric field at the image plane is

$$E(\xi) = \int_a^b e^{-ik\left(\frac{\tilde{\tilde{x}}}{f}\xi - P(x) + P_0 + y_0\right)} dx. \quad (24)$$

where $k = 2\pi/\lambda$ is the wave number. Substituting the first order expansions for \tilde{x} and $P(x)$, we get

$$\begin{aligned} E(\xi) &= \int_a^b e^{-ik\left(\frac{\tilde{x}(x)+(S(x,\tilde{x}(x))+g(\tilde{x}(x))A(\tilde{x}(x)))\theta}{f}\xi-x\theta\right)} dx \\ &= \int_{-\frac{d}{2}}^{\frac{d}{2}} e^{-ik\left(\frac{\tilde{x}+(S(x(\tilde{x}),\tilde{x})+g(\tilde{x})A(\tilde{x}))\theta}{f}\xi-x(\tilde{x})\theta\right)} A(\tilde{x}) d\tilde{x}. \end{aligned} \quad (25)$$

The second integral follows from the substitution $x = x(\tilde{x})$.

3.1. Recasting in Unitless Terms

To write the electric field using unitless quantities, we introduce θ , $\tilde{\theta}$, ξ , and \tilde{x} defined as follows:

$$\theta = \theta \frac{\lambda}{D}, \quad \tilde{\theta} = \tilde{\theta} \frac{\lambda}{d}, \quad \xi = \xi \frac{f\lambda}{d}, \quad \tilde{x} = \tilde{x}d \quad (26)$$

where $D = b - a$ denotes the aperture of the primary mirror. Each of these quantities is unitless. Associated with these changes of units, we introduce the following normalized versions of the apodization function, the transfer function, etc.:

$$\mathbf{A}(\tilde{x}) = A(\tilde{x}d)d/D \quad (27)$$

$$\mathbf{x}(\tilde{x}) = x(\tilde{x}d)/D \quad (28)$$

$$\mathbf{S}(\tilde{x}) = S(x(\tilde{x}d), \tilde{x}d)/D \quad (29)$$

$$\mathbf{g}(\tilde{x}) = g(\tilde{x}d)/d. \quad (30)$$

Making these substitutions, we get

$$E(\xi) = D \int_{-\frac{1}{2}}^{\frac{1}{2}} e^{-2\pi i\left(\tilde{x}\xi+(S(\tilde{x})+g(\tilde{x})\mathbf{A}(\tilde{x}))\frac{\lambda}{d}\theta\xi-\mathbf{x}(\tilde{x})\theta\right)} \mathbf{A}(\tilde{x}) d\tilde{x} \quad (31)$$

The term in the exponential with the λ/d factor is orders of magnitude smaller than the other terms, hence we drop it. The result is an explicit expression for the electric field in the image plane as a function of incidence angle θ , which is valid for small θ :

Theorem 3 To first order in θ , $E(\xi) = D \int_{-\frac{1}{2}}^{\frac{1}{2}} e^{-2\pi i(\tilde{x}\xi - \mathbf{x}(\tilde{x})\theta)} \mathbf{A}(\tilde{x}) d\tilde{x}$.

It is easy to check that the normalized apodization function is related to the normalized transfer function in the same way as before normalization:

$$\frac{d\mathbf{x}}{d\tilde{x}}(\tilde{x}) = \mathbf{A}(\tilde{x}). \quad (32)$$

Also, the domain of the $\mathbf{A}(\cdot)$ is $[-\frac{1}{2}, \frac{1}{2}]$ and it integrates to one.

The magnitude of the complex electric field is easy to compute if we assume that $\mathbf{A}(\cdot)$ is an even function. With this assumption, it follows that

$$\mathbf{x}(\tilde{x}) - \mathbf{x}(0) = \int_0^{\tilde{x}} \mathbf{A}(u) du \quad (33)$$

is an odd function. Hence,

$$E(\xi) = D e^{2\pi i \mathbf{x}(0)\theta} \int_{-\frac{1}{2}}^{\frac{1}{2}} \cos(2\pi(\tilde{x}\xi - (\mathbf{x}(\tilde{x}) - \mathbf{x}(0))\theta)) \mathbf{A}(\tilde{x}) d\tilde{x}. \quad (34)$$

The point-spread function (psf), which is the square of the magnitude of the electric field, is then given to first order by

$$\text{Psf}(\xi) = D^2 \left(\int_{-\frac{1}{2}}^{\frac{1}{2}} \cos(2\pi(\tilde{x}\xi - (\mathbf{x}(\tilde{x}) - \mathbf{x}(0))\theta)) \mathbf{A}(\tilde{x}) d\tilde{x} \right)^2. \quad (35)$$

3.2. Nonlinear Effects

If the expression $\mathbf{x}(\tilde{x}) - \mathbf{x}(0)$ is linear, then the off-axis psf is just a shift of the on-axis psf. Deviation from linearity, on the other hand, produces image degradation. One measure of such deviation is the rms phase error relative to $\mathbf{A}(0)$:

$$\text{Phase-Error} = \left(\int_{-\frac{1}{2}}^{\frac{1}{2}} (\mathbf{x}(\tilde{x}) - \mathbf{x}(0) - \mathbf{A}(0)\tilde{x})^2 d\tilde{x} \right)^{1/2}. \quad (36)$$

It is easy to check that the unitless first-order relationship between input angle θ and output angle $\tilde{\theta}$ is

$$\tilde{\theta} = \mathbf{A}(\tilde{x})\theta. \quad (37)$$

For a uniform apodization, $\mathbf{A}(\tilde{x}) = 1$ (see next section) and hence the unitless input and output angles match. However, for a nonuniform apodization, the unitless output angle depends on position across the pupil. On average, it equals the unitless input angle. But, the physical reality dictates using an amplitude weighted average rather than a simple average. In this case, the average unitless output angle is larger than the input angle:

$$\langle \tilde{\theta} \rangle = \int_{-\frac{1}{2}}^{\frac{1}{2}} \tilde{\theta} dx = \int_{-\frac{1}{2}}^{\frac{1}{2}} \tilde{\theta} \mathbf{A}(\tilde{x}) d\tilde{x} = \theta \int_{-\frac{1}{2}}^{\frac{1}{2}} \mathbf{A}(\tilde{x})^2 d\tilde{x} \geq \theta \quad (38)$$

(this last inequality follows from the Cauchy-Schwarz inequality and the fact that $\mathbf{A}(\tilde{x})$ integrates to one). For the types of apodizations arising in high-contrast imaging, the average unitless output angle can be more than twice as large as the input angle (see the numerical example in Section 5). This extra magnification is one of the attractive features of this approach to apodization.

4. Simple Examples

In this section, we consider a few simple examples.

4.1. Uniform Apodization

If the apodization function $A(\cdot)$ is a constant, call it A , then $x(\tilde{x}) = x_0 + A\tilde{x}$ and its inverse is $\tilde{x}(x) = (x - x_0)/A$. Plugging these into (9), we get that

$$h'(x) = \frac{(1 - \frac{1}{A})x + \frac{1}{A}x_0}{P_0} \quad (39)$$

$$g'(\tilde{x}) = \frac{x_0}{P_0} + \frac{A - 1}{P_0}\tilde{x} \quad (40)$$

and hence that each mirror is parabolic. In the special case where $A = 1$, the two mirrors are actually planar and the system is a simple *periscope*. For $A \neq 1$, the differential equations integrate as follows:

$$h(x) = c + \frac{(x - \xi)^2}{4H} - \frac{P_0}{2} \quad (41)$$

$$g(\tilde{x}) = c + \frac{(\tilde{x} - \xi)^2}{4G} \quad (42)$$

where c is an arbitrary constant of integration, $\xi = -x(0)/(A - 1)$ is the x -coordinate of the centerline of the system, $H = AP_0/(2(A - 1))$ is the focal length of the “ h ” mirror, and $G = P_0/(2(A - 1))$ is the focal length of the “ g ” mirror. Note that $H = AG$ and hence that the magnification of the system is A . Using the fact that $A = D/d$, the normalized apodization function is

$$A(\tilde{x}) = A(\tilde{x}d) \frac{d}{D} = Ad/D = 1 \quad (43)$$

and the normalized transfer function is

$$x(\tilde{x}) = \frac{x(\tilde{x}d)}{D} = \frac{x_0}{D} + \tilde{x}. \quad (44)$$

Since $x(\tilde{x})$ depends linearly on \tilde{x} , it follows that the off-axis point-spread function is just a shift of the on-axis psf:

$$\text{Psf}(\xi) = D^2 \left(\int_{-\frac{1}{2}}^{\frac{1}{2}} \cos(2\pi\tilde{x}(\xi - \theta)) d\tilde{x} \right)^2. \quad (45)$$

Of course, in practice such a pair of parabolic mirrors will exhibit off-axis errors beyond just a shift of the psf but these errors can only be captured by a second-order (or higher) analysis.

4.2. A Cosine Apodization

A simple explicit apodization function that approximates the sort of smoothly tapering apodizations needed for high-contrast imaging is given by the cosine function:

$$A(\tilde{x}) = a \left(1 + \cos \frac{2\pi\tilde{x}}{d} \right). \quad (46)$$

For this case, the transfer function $x(\tilde{x})$ is given by

$$x(\tilde{x}) = x(0) + a\tilde{x} + a \frac{d}{2\pi} \sin \frac{2\pi\tilde{x}}{d} \quad (47)$$

and the “ g ” mirror’s surface is given by

$$g(\tilde{x}) = c + \frac{x(0)\tilde{x} + \frac{a-1}{2}\tilde{x}^2 - a \frac{d^2}{4\pi^2} \cos(2\pi\tilde{x})}{P_0}. \quad (48)$$

The expression for the “ h ” mirror’s surface can be given explicitly using (10) and the inverse of $x(\tilde{x})$ but it is messy so we don’t record it here. The amplitude parameter a determines the relationship between d and D :

$$\frac{D}{2} = x\left(\frac{d}{2}\right) - x(0) = a \frac{d}{2} \quad \implies \quad D = ad. \quad (49)$$

The normalized apodization is

$$\mathbf{A}(\tilde{\mathbf{x}}) = 1 + \cos(2\pi\tilde{\mathbf{x}}) \quad (50)$$

and the normalized transfer function is

$$\mathbf{x}(\tilde{\mathbf{x}}) = \frac{x_0}{D} + \tilde{\mathbf{x}} + \frac{1}{2\pi} \sin(2\pi\tilde{\mathbf{x}}). \quad (51)$$

The nonlinearity of the transfer function implies a nontrivial transformation in addition to the usual shift of the off-axis psf:

$$\text{Psf}(\boldsymbol{\xi}) = D^2 \left(\int_{-\frac{1}{2}}^{\frac{1}{2}} \cos(2\pi\tilde{\mathbf{x}}(\boldsymbol{\xi} - \boldsymbol{\theta}) - \boldsymbol{\theta} \sin(2\pi\tilde{\mathbf{x}})) \mathbf{A}(\tilde{\mathbf{x}}) d\tilde{\mathbf{x}} \right)^2. \quad (52)$$

In the next section, we consider a similar smooth apodization and plot some of the off-axis psf's to see explicitly the impact of this nonlinear effect.

5. A Numerical Example

The apodization function shown in Figure 3 has unit area and provides 10^{-10} contrast from $4\lambda/D$ to $60\lambda/D$. It was computed using the methods given in Vanderbei et al. (2003). The on-axis point spread function, computed by setting $\boldsymbol{\theta} = 0$ in (35) is shown in Figure 4.

In a solar-like system, a star's diameter is about 0.01au. Hence, if a 1au Earth-like planet appears from Earth at $5\lambda/D$, then the angular extent of the star would be from $-0.025\lambda/D$ to $0.025\lambda/D$. Therefore, starlight will enter the system from angle $\boldsymbol{\theta} = 0.02\lambda/D$. The psf associated with this slightly off-axis starlight is shown in Figure 5. Although it is not possible to see it from the figure, the threshold for high contrast, i.e. 10^{-10} , is pushed to $6.0\lambda/D$. Thresholds for high-contrast associated with other values of $\boldsymbol{\theta}$ are shown in Table 1. It is clear from this table that non-zero stellar size and pointing error increase the inner working angle to at least $6\lambda/D$.

The psf's associated with a planet at 5 and 10 λ/D are shown in Figures 6 and 7. Note that the magnification due to nonlinearity, described at the end of Section 3, is clearly evident. For example, in Figure 6, the input angle is $5\lambda/D$ but the peak of the psf occurs at about $12\lambda/D$. Hence, there is a magnification by more than a factor of two.

On the other hand, the unsharpening of the psf's and the corresponding reduction in peak value suggest that a contrast level of 10^{-10} for the on-axis case might not be sufficient for planet detection using only the two-mirror system discussed here. Guyon (2003) suggests that an additional set of

two mirrors can be used to restore the off-axis (planet) images with good fidelity. The detailed investigation of this addition to the optics will be investigated in a future paper.

Acknowledgements. We would like to express our gratitude to N.J. Kasdin, D.N. Spergel, and E. Turner for the many enjoyable and stimulating discussions in regard to this work. In particular, N.J. Kasdin read several drafts carefully and provided helpful advice as we struggled with various parts of this paper. This research was partially performed for the Jet Propulsion Laboratory, California Institute of Technology, sponsored by the National Aeronautics and Space Administration as part of the TPF architecture studies and also under contract number 1240729. The second author received support from the NSF (CCR-0098040) and the ONR (N00014-98-1-0036).

REFERENCES

- A. Goncharov, M. Owner-Petersen, and D. Puryayev. Apodization effect in a compact two-mirror system with a spherical primary mirror. *Opt. Eng.*, 41(12):3111, 2002.
- O. Guyon. Phase-induced amplitude apodization of telescope pupils for extrasolar terrestrial planet imaging. *Astronomy and Astrophysics*, 404:379–387, 2003.
- A. Labeyrie. Resolved imaging of extra-solar planets with future 10-100km optical interferometric arrays. *Astronomy and Astrophysics*, 118:517, 1996.
- W.A. Traub. Combining beams from separated telescopes. *Applied Optics*, 25:528–532, 1986.
- R.J. Vanderbei, D.N. Spergel, and N.J. Kasdin. Circularly Symmetric Apodization via Starshaped Masks. *Astrophysical Journal*, 2003. Submitted.

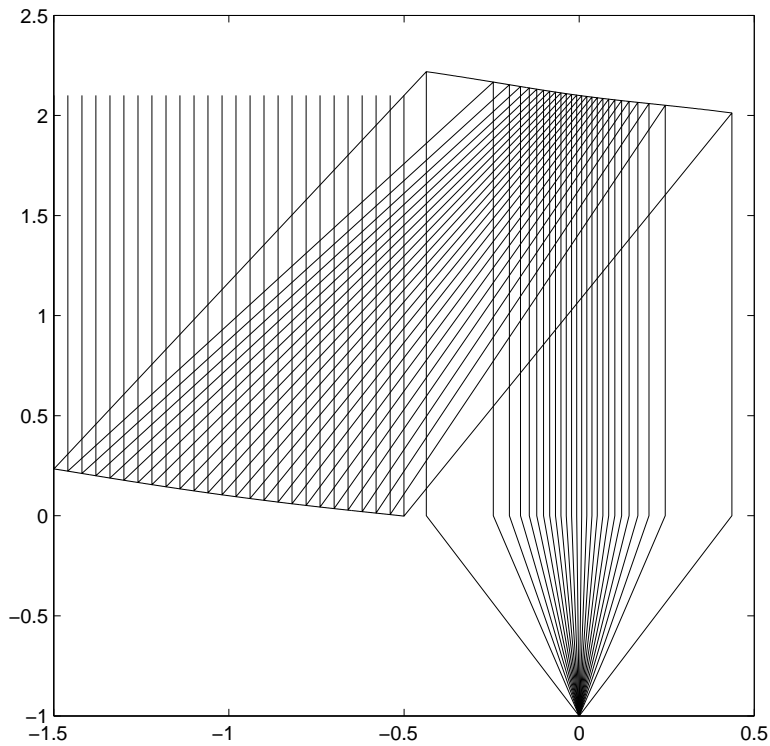


Fig. 1.— Parallel light rays come down from above, reflect off the bottom mirror (on the left), bounce up to the top mirror (on the right), and then exit downward as a parallel bundle with a concentration of rays in the center of the bundle and thinning out toward the edges—that is, the exit bundle is apodized. A focusing element on the x -axis then creates an image.

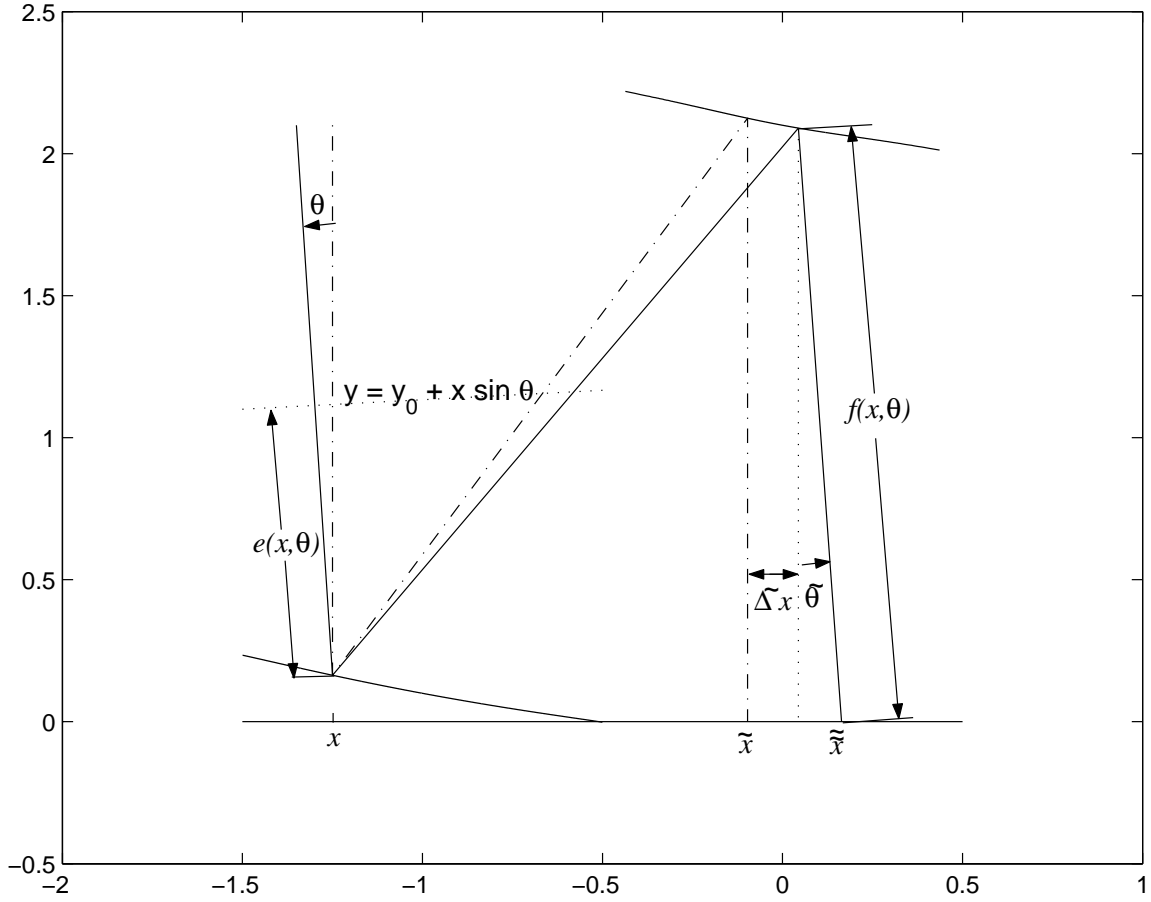


Fig. 2.— Notations for off-axis expressions. Parallel light rays come down at an angle θ from vertical, reflect off the bottom mirror (on the left), bounce up to the top mirror (on the right), and then exit downward at an angle $\tilde{\theta}$ hitting the x -axis at a new location \tilde{x} .

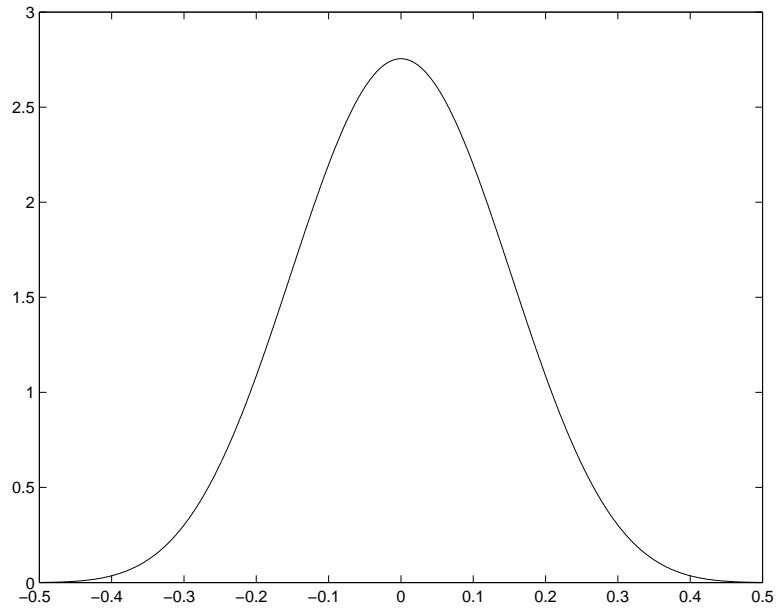


Fig. 3.— A unit area apodization providing contrast of 10^{-10} from $4\lambda/D$ to $60\lambda/D$.

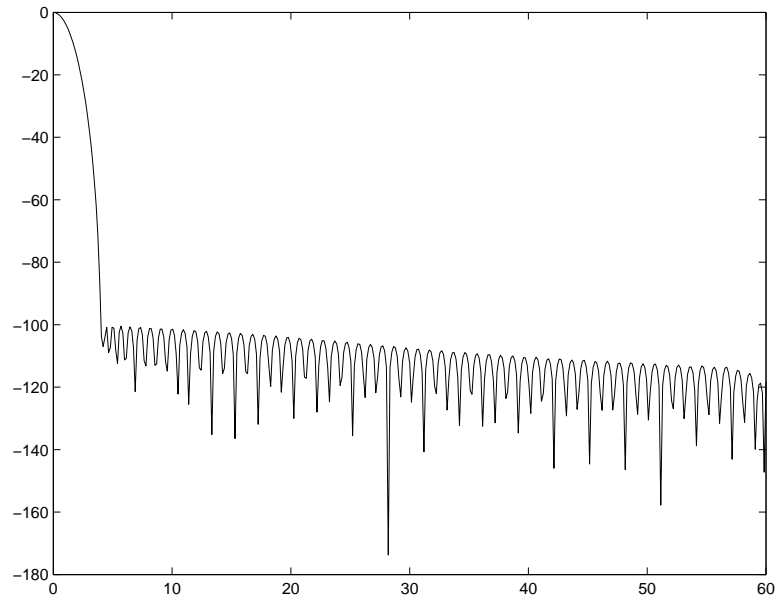


Fig. 4.— The on-axis point spread function for the apodization shown in Figure 3.

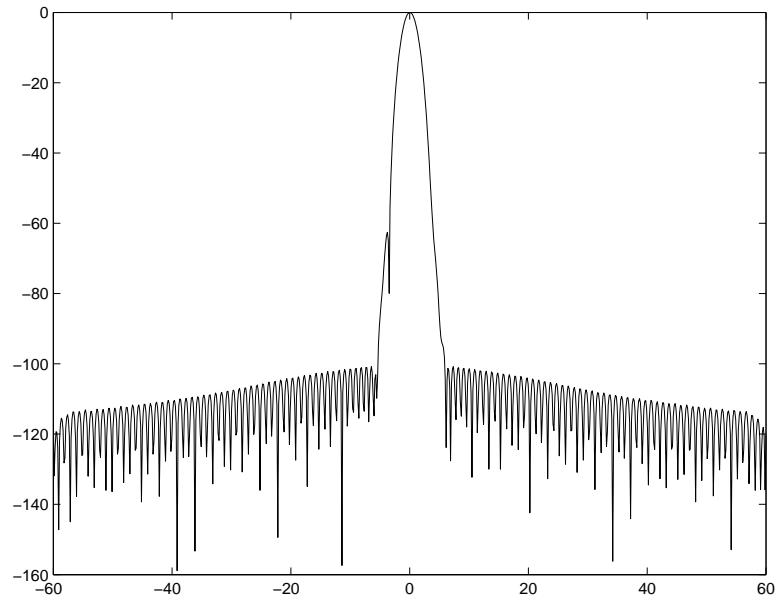


Fig. 5.— The off-axis point spread function for the apodization shown in Figure 3 computed at $\theta = 0.02\lambda/D$.

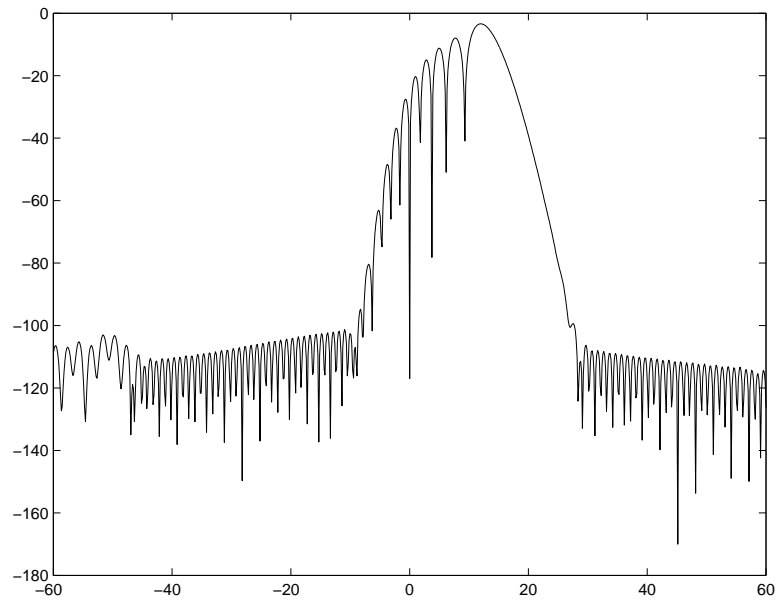


Fig. 6.— The off-axis point spread function for the apodization shown in Figure 3 computed at $\theta = 5\lambda/D$. Note that the main lobe appears at $12\lambda/D$. The nonuniformity of the apodization accounts for both the spreading out of the point spread function as well as the apparent magnification by a factor of $12/5 = 2.4$.

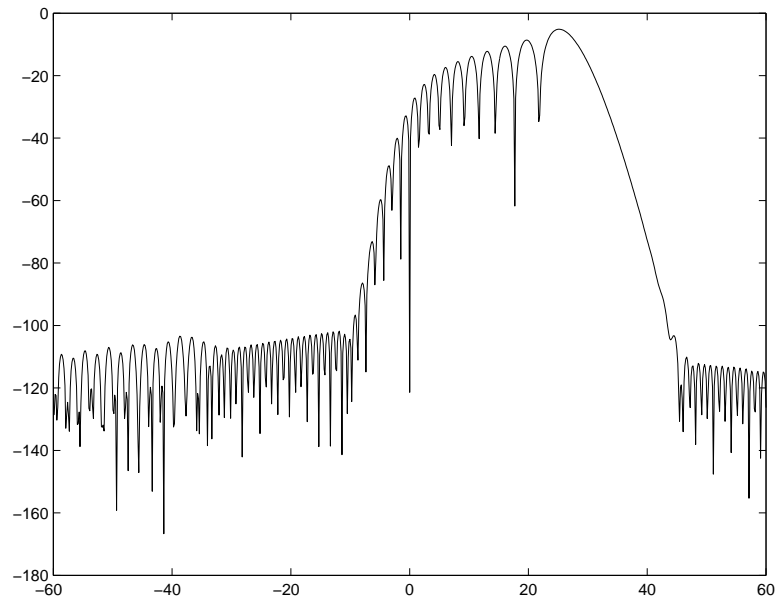


Fig. 7.— The off-axis point spread function for the apodization shown in Figure 3 computed at $\theta = 10\lambda/D$. Note that the main lobe appears at about $22\lambda/D$ for an effective magnification of about 2.2.

Sky	Focal Plane			
θ	Contrast threshold	angle of peak intensity		effective angular
λ/D	λ/D	λ/D		magnification λ/D
0.00	4.0	-4.0	0.0	
0.01	5.2	-5.2	0.023	2.3
0.02	6.0	-5.2	0.045	2.3
0.10	6.4	-6.0	0.23	2.3
0.50	9.9	-6.6	1.05	2.1
2.00	15.9	-7.7	4.35	2.2
5.00	27.0	-8.5	12.0	2.4
10.00	43.5	-9.3	25.2	2.5

Table 1: Output image properties as a function of input angle. Column 1 is the input angle on the sky of a point source. Columns 2 and 3 are the output angles at which the intensity in the focal plane falls to 10^{-10} compared to the on-axis image peak. Column 4 is the output angle at which the star image has its peak intensity. Column 5 is the effective angular magnification factor, i.e., the ratio of column 4 to column 1.